actuators

MDPI

Article

TacFR-Gripper: A Reconfigurable Fin-Ray-Based Gripper with Tactile Skin for In-Hand Manipulation

Qingzheng Cong, Wen Fan and Dandan Zhang *

Department of Bioengineering, Imperial College London, and the I-X Initiative, London SW7 2BX, UK; qcong@ic.ac.uk (Q.C.); w.fan24@imperial.ac.uk (W.F.)
* Correspondence: d.zhang17@imperial.ac.uk

Abstract: This paper introduces the TacFR-Gripper, a novel reconfigurable soft robotic gripper inspired by the Fin-Ray effect and equipped with tactile skin. The gripper incorporates a four-bar mechanism for accurate finger bending and a reconfigurable design to change the relative positions between the fingers and palm, enabling precise and adaptable object grasping. This 5-Degree-of-Freedom (DOF) soft gripper can facilitate dexterous manipulation of objects with diverse shapes and stiffness and is beneficial to the safe and efficient grasping of delicate objects. An array of Force Sensitive Resistor (FSR) sensors is embedded within each robotic fingertip to serve as the tactile skin, enabling the robot to perceive contact information during manipulation. Moreover, we implemented a threshold-based tactile perception approach to enable reliable grasping without accidental slip or excessive force. To verify the effectiveness of the TacFR-Gripper, we provide detailed workspace analysis to evaluate its grasping performance and conducted three experiments, including (i) assessing the grasp success rate across various everyday objects through different finger configurations, (ii) verifying the effectiveness of tactile skin with different control strategies in grasping, and (iii) evaluating the in-hand manipulation capabilities through object pose control. The experimental results indicate that the TacFR-Gripper can grasp a wide range of complex-shaped objects with a high success rate and deliver dexterous in-hand manipulation. Additionally, the integration of tactile skin is demonstrated to enhance grasp stability by incorporating tactile feedback during manipulations.

Keywords: in-hand manipulation; tactile perception; soft robotic hand

check for updates

Citation: Cong, Q.; Fan, W.; Zhang, D. TacFR-Gripper: A Reconfigurable Fin-Ray-Based Gripper with Tactile Skin for In-Hand Manipulation. *Actuators* **2024**, *13*, 521. https://doi.org/10.3390/act13120521

Academic Editor: Matteo Cianchetti

Received: 31 October 2024
Revised: 6 December 2024
Accepted: 13 December 2024
Published: 17 December 2024

Copyright: © 2024 by the authors. Licensee MDPI, Basel, Switzerland. This article is an open access article distributed under the terms and conditions of the Creative Commons Attribution (CC BY) license (https://creativecommons.org/licenses/by/4.0/).

1. Introduction

In recent years, soft and compliant robotic grippers have captured increasing attention by offering high flexibility, adaptability, and safety compared to traditional rigid grippers [1,2]. For example, the Fin-Ray-based robotic gripper draws inspiration from the fin movements of fish to deliver a versatile and effective gripping mechanism [3]. With impressive flexibility, it can easily adapt to an object's contours, thus providing a greater contact area for grasping [4**?** –6]. However, most of the existing Fin-Ray-based soft robotic grippers lack tactile perception and in-hand manipulation functions, resulting in limited accuracy for grasping, and neither can they adjust an object's poses within the robotic hand [3,8,9]. Therefore, we aim to design a Fin-Ray-based reconfigurable robotic gripper integrated with tactile sensors, which can be used for dexterous in-hand manipulation tasks.

Recent advancements in soft robotic grippers, exemplified by the Belt-Augmented Compliant Hand (BACH) [10], have shed light on Fin-Ray-based soft grippers for in-hand manipulation. BACH, leveraging a timing belt integrated around a compliant Fin-Ray-based finger architecture, can achieve in-hand manipulation via power grasp. However, the lack of active surfaces and reconfigurable ability of the palm restricts its capacity to handle objects of a wide range of sizes and shapes, especially those with irregular shapes that are too small or too large relative to the gripper. Such a timing belt for manipulation

limits the weight of the handleable objects and introduces potential robustness issues and decreased energy efficiency due to reliance on friction and sliding motions. Moreover, it does not incorporate tactile sensing for feedback control.

To this end, our research aims to design a reconfigurable Fin-Ray-based robotic gripper with more active joints for dexterous in-hand manipulation, while enhancing the precision of control by using a four-bar mechanism for finger bending motion control. Tactile skin, which comprises an array of sensing elements, is integrated into each fingertip to allow the gripper to perceive contact information during manipulation and adjust its grip accordingly.

In summary, the contributions of our study are listed as follows:

- We develop a 5-DOF Fin-Ray-based robotic gripper utilizing the 3D printing technique, which incorporates a four-bar mechanism for precise finger movement control and features a reconfigurable mechanism in the palm. This design enables dexterous in-hand manipulation with support from extensive degrees of freedom, allowing for adaptable interaction with a variety of objects.
- Integration of the aforementioned robotic gripper design with tactile skin to enhance the perception of contact force and better gripping force control.

2. Related Work

2.1. Soft Robotic Gripper with Tactile Sensing

Tactile sensing in soft robotic grippers can help improve object manipulation reliability by providing direct contact information, which is crucial for precise in-hand manipulation and feedback control.

Sakuma et al. developed a granular-jamming-based universal soft gripper [11] with transparent filling. This gripper included an internal camera to trace markers on its surface, enabling a 3D reconstruction of the contact surface. An optical tactile palm integrated with a soft gripper was developed by Xuyang [12], which enables stable and precise grasping and placement of fragile objects through functions like light contact detection, grasp pose adjustment, and loss-of-contact detection. A soft gripper named TaTa [13] incorporates RGB tricolor LEDs and employs an inbuilt camera to monitor color changes on the contact surface, significantly enhancing the resolution of the tactile image. However, integrating rigid elements such as camera modules, circuit boards, and lights into soft fingers without influencing the soft gripper's active deformation poses a challenge. Zhao et al. introduced GelSight Svelte [14], a soft, finger-sized device that employs a camera to capture the reflection from a curved mirror, providing proprioceptive and tactile information. However, the GelSight Svelte design is limited by its lack of compliant properties. In Chen's work, compact strain-gauge sensors are integrated into the beam of the Fin-Ray finger, making the gripper able to control the contact force between objects within around 5% RMS error [15].

Liu et al. equipped a Fin-Ray-based finger with the GelSight tactile sensor [16], enabling the detection of an object's pose and facilitating tactile reconstruction. This setup proved effective for reorienting a glass jar [17]. However, the delicate nature of the GelSight sensor, tightly integrated with the finger's structure, poses durability concerns. Wear and tear, such as tearing at the skin's connection to the housing or elastomer shearing from intensive manipulation or collisions, can damage the sensor. These issues potentially limit the gripper's service life and reduce its cost-effectiveness.

Although tactile sensor arrays may exhibit drawbacks like relatively low resolution compared to vision-based tactile sensors [18–20], they have inherent advantages in terms of design flexibility and easy integration to a diverse range of robotic hands. In Yang et al.'s work [21], they developed a monolithic tendon-driven, Fin-Ray-inspired gripper integrated with a pressure film sensor along the entire side of the finger. This design significantly enhanced the gripper's ability to sense forces, allowing it to handle more delicate and fragile objects with precision. Similarly, Kaiwen et al. [22] implemented FSR sensors distributed across the three-finger Fin-Ray gripper for slip detection and force control. In their experiments of apple harvesting, this approach reduced damage to apples to 0% while maintaining a high success rate of 80% in harvesting. Based on soft and thin characteristics,

tactile sensor arrays facilitate seamless integration into robotic systems, especially for tasks requiring compact and conformable designs such as Fin Ray. Additionally, their rapid response time enables real-time adjustments during complex interactions such as force control, making them particularly suited for dexterous robotic applications.

2.2. Reconfigurable Soft Gripper for In-Hand Manipulation

The reconfigurable soft gripper marks a significant advancement in the field of robotics, especially for in-hand manipulation, which needs to delicately handle a wide array of objects with varying shapes and sizes.

A versatile soft robotic gripper was developed with three 3D-printed soft pneumatic actuators and a reconfigurable design [23]. It can transform between various configurations for grasping, including scoop, pinch, and claw configurations. Operating each finger independently brings its advantages in grasping diverse objects and performing intricate in-hand manipulations. However, when compared to Fin-Ray-based designs, this gripper exhibits reduced strength, limiting the weight of objects it can securely grasp. Also, the inherent characteristics of the soft pneumatic actuators constrains its control precision. Furthermore, it cannot conduct dexterous in-hand manipulation due to the limited DOFs. An active elastic band-based gripper was created by Sheng's team [24], capable of compliant grasping and in-hand manipulation using adaptive wrapping and conveyor motion. Li designed a soft robotic finger with a soft polyhedral structure with 3D omni-adaptability and an active surface [25], demonstrating stability and dexterity for the in-hand manipulation of irregular shaped objects. In Wang's work, a reconfigurable gripper was developed that can switch between rigid, rigid bending, and flexible states, enhancing adaptability for diverse tasks [26].

Batsuren et al. focused on a gripper with three pneumatic fingers [27], each containing three air chambers: two for twisting in different directions and one for grasping. This design enables the gripper to handle objects of varying shapes and sizes. This design was later improved by inserting a stiff rod that can be manoeuvred inside the central hole of each finger to control the bending point [28]. This new configuration significantly enhances the dexterous grasping capabilities of the soft gripper, with a specific emphasis on in-hand manipulations. Jain et al. developed a gripper equipped with retractable fingernails and a versatile active palm [29], which enables the grasping of objects with various geometries, sizes, and weights.

The above grippers perform well in grasping tasks, showcasing adaptability to various object shapes and sizes. However, they are inherently limited in Degree-of-Freedom (DOF) compared to the design discussed in this paper, which could affect their potential for in-hand manipulation. Some of these grippers also lack tactile sensing capabilities, which may lead to challenges in maintaining delicate object handling, such as avoiding slippage or excessive force application. Consequently, while effective, they may have slightly less potential for highly dexterous, precise manipulations.

3. Materials & Methods

3.1. Hardware Design

3.1.1. Robot Gripper Design

The gripper consists of four main components: three Fin-Ray-based robotic fingers, three four-bar mechanisms for controlling finger bending motion, three ST-802 mini linear actuators, and a palm equipped with two MG995 servo motors to reposition the side fingers relative to the palm (see Figure 1b). Each finger of the robotic gripper has a width of 30 mm and a height of 101 mm. The maximum distance between the two side fingers is 110 mm, which constitutes Configuration 1, as shown in Figure 2c.

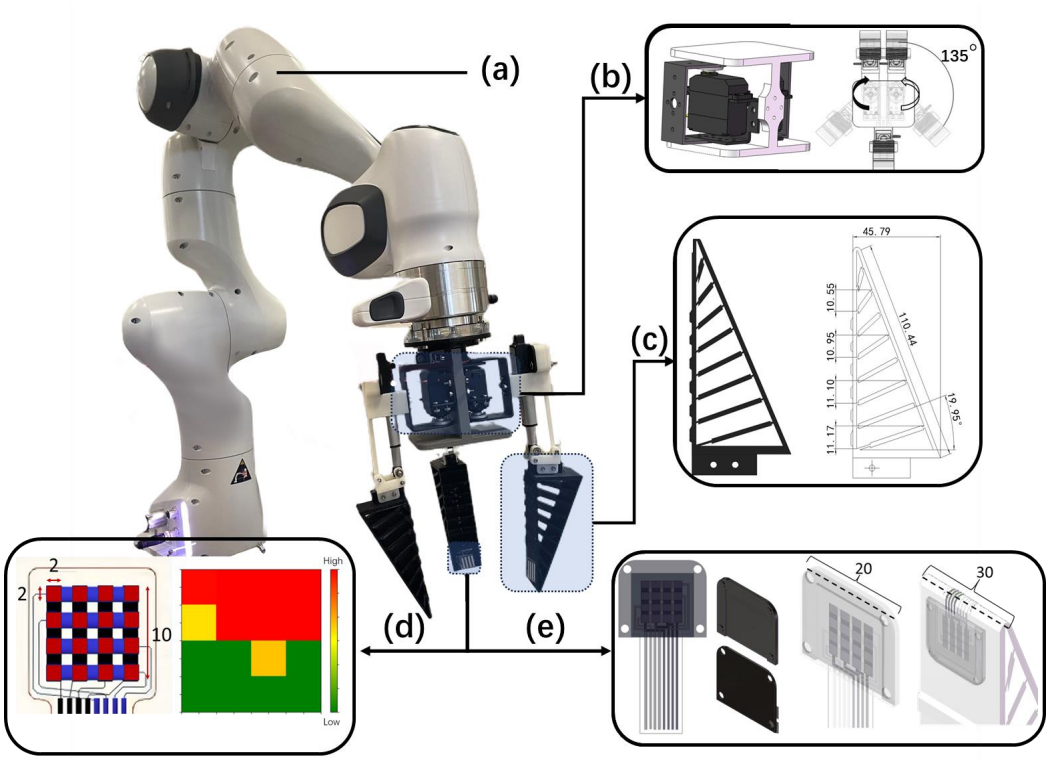


Figure 1. Overviewdesign of the soft gripper with tactile feedback. (**a**) Franka Emika Robot. (**b**) Reconfigurable base driven by servo motors, which enable the side finger of the gripper to have a 135-degree rotational range. (**c**) Fin-Ray-based finger and its specific design parameter. (**d**) Tactile skin and visualization of the tactile image obtained by the embedded FSR sensor in the tactile skin. (**e**) Demonstration of the FSR and its skin integration with the Fin-Ray-based finger. (All units in this graph are in mm).

The reconfiguration of the gripper is enabled by two servo motors assembled in the hollow area of the palm, which grant rotational movement to the side fingers (see Figure 1b). As illustrated in Figure 2c, the robotic gripper can flexibly adjust its gestures into three general configurations. Configuration 1 engages solely in using the side fingers to grasp targeted objects. Configuration 2 involves the collaborative effort of all three fingers, making it suitable for grasping objects with spherical shapes. Configuration 3 is used for grasping elongated objects in a horizontal position. See the supplementary material for visual representations of grasping with different configurations.

The Fin-Ray-based fingers are 3D printed with Thermoplastic Polyurethane (TPU) with 95A Shore Hardness. This material can ensure a secure grip by closely conforming to various objects while retaining enough stiffness for effective force application. It significantly enhances the adaptability of robotic grippers to conform to different shapes, thereby substantially increasing the contact area between the gripper and the object. This natural deformation allows the fingers to adapt to the object's surface shape during grasping, providing a degree of self-control in the grip in case of exceeding force. This is particularly beneficial when handling delicate objects. Additionally, TPU's impressive resilience, demonstrated by its high elastic limit, makes it well-suited for long-term, repetitive gripping tasks in robotic applications. However, this adaptation is not precise, as it relies on the passive compliance of the material and the Fin-Ray structure rather than active adjustment. To address this limitation, an FSR sensor is integrated into the fingertip for closed-loop control, so this system can have more precise control over the grip. The structure of the Fin-Ray-based finger is also modified by increasing the crossbeam angle from 10 to 70 degrees (top to bottom) gradually for a better larger deformation when grasping [30]. The width

of the finger is increased to 3 cm for a larger polar moment of inertia of 2.3×10^6 mm^4 to resist twisting during the grasping.

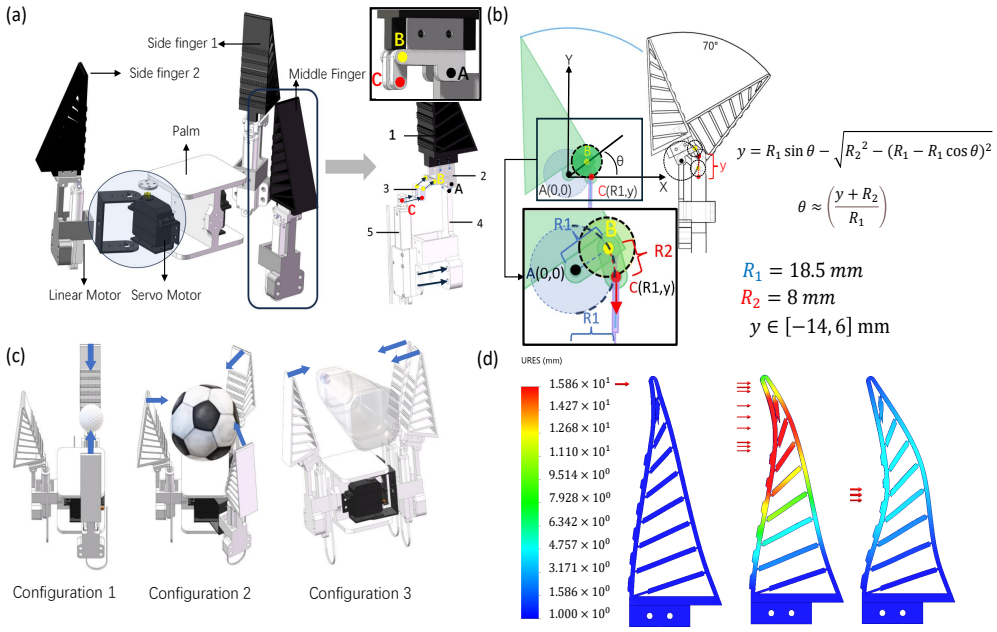


Figure 2. Hardware overview. (**a**) The detailed mechanical structure of TacFR is illustrated, showcasing side fingers 1 and 2, the middle finger, palm, linear motor, and servo motor, all assembled on the TacFR gripper. Additionally, an exploded view of the robotic gripper is presented, highlighting the 3D-printed components (1, 2, 3, 4), a four-bar mechanism, and a linear actuator (5). The kinematic diagram of the finger's range of motion is also included, where Point A is fixed at the top endpoint of Component 4, connecting to the bottom endpoint of Component 2 (Fin-Ray bottom connection part). Point B represents the other bottom endpoint of Component 2, which connects to Component 3, while Point C corresponds to the top endpoint of Component 5 (linear actuator), connecting to the other end of Component 3. The assembled components are depicted above the exploded view, with Points A, B, and C clearly labelled for clarity. (**b**) Kinematic diagram of the finger's range of motion, with R1 and R2 denoting pivot radii, and 'y' representing the linear actuator's endpoint displacement. θ indicates the finger's bend angle. (**c**) Illustrative configurations of the gripper that demonstrate parallel, trigonal, and T-shaped grasps. (**d**) The finite element analysis of the Fin-Ray-based finger's relative movement in the X direction under different contact locations.

In the finite element analysis shown in Figure 2d, a modified Fin-Ray structure made with TPU was tested using the following material properties: Elastic Modulus $E = 150$ MPa, Poisson's Ratio $\nu = 0.45$, Mass Density $\rho = 1235\,\mathrm{kg/m^3}$, and Yield Strength $\sigma_y = 35$ MPa. Under a 100 N applied force, the response varies based on the contact point on the structure.

When force is applied at the tip, the horizontal displacement remains minimal, which is advantageous for precisely handling small objects by concentrating force in a confined area. Conversely, applying force at the middle of the finger results in a larger horizontal displacement, allowing it to better adapt to an object's shape and distribute pressure evenly for a gentler grip. The back end, which has a rough surface to increase friction, shows a moderate horizontal displacement. It is well-suited for grasping larger, heavier objects by enhancing control and force transmission. The FEM simulation result visualizations, can be found in the Supplementary Materials.

3.1.2. Gripper Kinematic Model

Figure 2a,b illustrates the mechanical structure of the proposed robotic gripper and displays the kinematic diagram of the finger and its motion range. The kinematic diagram

showcases the relationship between the linear actuator's displacement and the Fin Ray's bending angle, which is shown below as Equation (1).

$$y = R_1 \sin\theta - \sqrt{R_2^2 - (R_1 - R_1 \cos\theta)^2} \tag{1}$$

where:

- y is the vertical displacement of the end of the linear actuator (Point C); it ranges from -14 to 6 mm relative to point A in the Y direction.
- R_1 is the displacement between the two installation holes of Component 2 (Displacement between Point A B).
- R_2 is the displacement between the two installation holes of Component 3 (Displacement between Point C B), and the distance between points C and A in the X direction.
- θ is the bending angle of the finger ($\angle BAX$ shown in Figure 2b).

By applying first-order Taylor expansion approximation to this formula, the bending angle can be expressed by the linear actuator's displacement as Equation (2):

$$\theta \approx \left(\frac{y + R_2}{R_1}\right) \cdot \frac{180}{\pi} = \left(\frac{y + 8}{18.5}\right) \cdot \frac{180}{\pi} \tag{2}$$

By comparing the original and approximation functions' values within the desired range, and calculating the Mean Percentage Error for each value, the average relative error between the first-order Taylor expansion approximation and the actual kinematic formula is obtained, which is 0.735%. This supports the effectiveness of the linear relationship approximation, which simplifies the design of control systems, reduces the need for complex nonlinear compensation, and makes the system easier to quantify and describe since the movement of the linear actuator is almost linearly proportional to the finger's bending angle.

3.2. Workspace Analysis

Workspace analysis is crucial in robotics for understanding the capabilities of robotic manipulators or grippers for manipulation [31–33]. In this work, "dexterity" refers to the capability of the gripper to successfully grasp and manipulate objects of varying sizes within a specific region of its workspace. Higher dexterity indicates that the gripper can more stably grasp objects in that area, whereas lower dexterity suggests reduced control and efficiency. In this work, we iteratively generate a large number of potential finger contact locations based on the gripper's specific kinematic configurations. This approach not only highlights the accessibility of the robot's fingers but also enables a thorough exploration of the gripper's workspace. Unlike the stochastic point generation seen in the Monte Carlo method, our strategy ensures a more systematic and even coverage [34,35].

Figure 3a displays the potential contact points between the gripper's three fingers and the targeted object for grasping. Assuming that all objects are spherical and that only three contact points (one from each finger's point cloud) will make contact with the object. Upon establishing the coordinates of these three contact points, we can generate the direction of the force from each point, oriented perpendicularly to the finger's inner surface. By iteratively increasing the force exerted at each contact point in its specific direction, we can obtain the minimum resultant forces and torque for each point combination. An object is considered graspable if both the resultant force and torque remain beneath a predetermined threshold affected by the frictional forces and the potential deformation of the fingers, specifically set at 5% of the object's weight for both force and torque. These thresholds account for frictional forces and potential deformation of the fingers, ensuring that the grasp can accommodate minor external disturbances while maintaining stability.

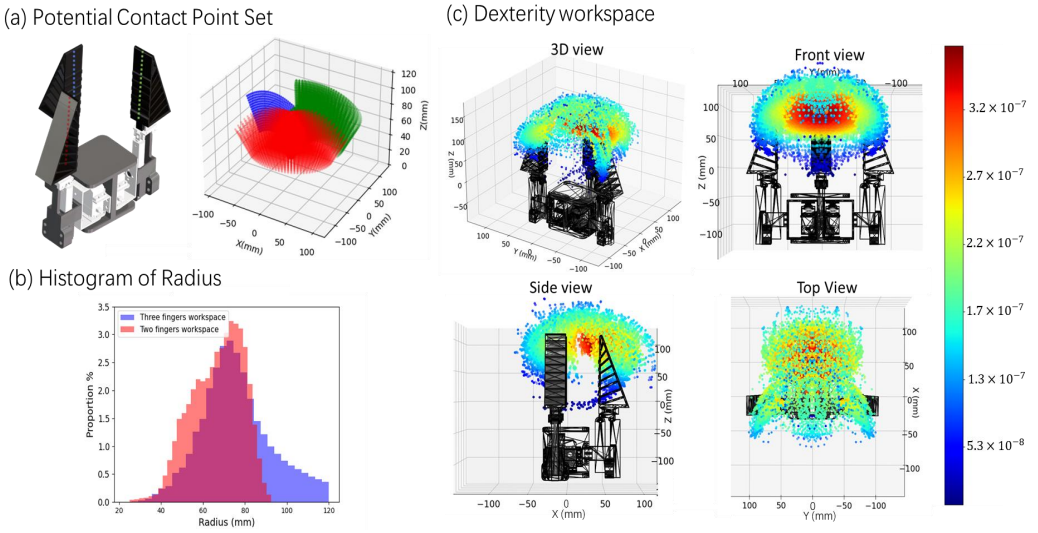


Figure 3. (**a**) Visualization of the reachable workspace analysis for a gripper based on point-cloud-based simulation. (**b**) Histograms showing the distribution of circumradius for Configuration 1 (red) and Configurations 2 and 3 (blue), indicating the overall trend of graspable object sizes. (**c**) 3D view of the dexterous workspace for Configurations 2 and 3 and its views along the X, Y, and Z axes for objects with a radius between 90 and 95 mm.

Furthermore, we calculate the circumradius of triangles defined by the points of contact on spherical objects. This circumradius directly corresponds to the sphere's radius, providing a measure of the object's size. Utilizing this radius, we construct a histogram that illustrates the gripper's dexterity with objects of specific dimensions within its total grasping range. This visual representation enables us to assess the gripper's efficacy in handling a spectrum of object sizes, highlighting its versatility. In Figure 3b, the red area illustrates Configuration 1, which is designed for grasping smaller objects using a pinching method. The blue area of the same figure represents Configurations 2 and 3, demonstrating the gripper's capability to handle medium and large-sized objects, specifically those with a radius ranging from 60 to 80 mm.

For dexterous workspace analysis, Kernel Density Estimation (KDE) with a Gaussian kernel is utilized to create smooth, continuous density estimations [36] based on discrete successful grasp, which illustrates the regions where the gripper is most dexterous at handling objects of various sizes. The formula for the Gaussian kernel density estimate is shown below as Formulas (3) and (4).

$$f(x) = \frac{1}{n \cdot h} \sum_{i=1}^{n} K\left(\frac{x - x_i}{h}\right) \tag{3}$$

$$K(u) = \frac{1}{\sqrt{2\pi}} e^{-\frac{1}{2}u^2} \tag{4}$$

where:

- $f(x)$ is the estimated density at point x. It represents the likelihood of successful grasps at point x in the workspace.
- n is the number of data points.
- h is the bandwidth; it is set as 'silverman', which controls the width of the kernel, thus controlling the smoothness of the density estimation. In our case, this achieves a balance between smoothness and preserving important details of the gripper's dexterity across the workspace.
- u is the standardized distance $(x - x_i)/h$, where the value represents the relative position from chosen point x to all other points x_i, adjusted by the bandwidth h.

- $K(u)$ assigns weights to data points based on their distance from x. In this case, we use the Gaussian kernel, which has a bell-shaped curve, meaning that data points closer to x have a greater influence (higher weight), while distant points have less influence.

In Figure 3c, the dexterous workspace analysis and visualization of the gripper for grasping objects with varying radii (from 90 mm to 95 mm) is shown. Darker shades like blue indicate lower dexterity, while brighter regions (reds and yellows) indicate higher dexterity. Each view provides a unique angle, offering a comprehensive understanding of the gripper's capabilities and limitations in manipulating objects of selected radius range. However, when manipulating objects with a radius of 110–120 mm, the gripper's workspace features two highly dexterous regions on both sides. These regions are separated by an area with lower dexterity, indicating a gap in the dexterity workspace for objects transitioning between them. For larger objects, the workspace lacks such a gap but is rather confined and concentrated within a limited area.

For dexterity analysis, unlike conventional methods that define dexterity based on the reachable positions of the end effector, our approach defines dexterity by evaluating the gripper's ability to successfully grasp objects of varying sizes and specific positions, providing a more object-centric measure of the gripper's dexterity.

In summary, by using the dexterity workspace with potential contact point generation and Gaussian kernel density estimate can obtain the spatial distribution and the effective dexterity that the robotic gripper can achieve in its operational environment. In this way, the dexterity level of the gripper's kinematic structure can be quantified for further optimization. This distribution can also aid in precise task planning and ensures safer, more efficient interactions in automated environments.

Sensor Integration and Calibration

As illustrated in Figure 1d, the tactile array has a total sensing area of 10 mm $\times$ 10 mm. Within this area, the sensing elements are arranged in a 4 $\times$ 4 grid, resulting in a total of 16 individual sensing units, or pixels. Each pixel measures 2 mm $\times$ 2 mm, contributing to an effective sensing area of 4 mm^2 per pixel. When combined, the active sensing area accounts for 64% of the total tactile array. As illustrated in Figure 1e, two soft skins are 3D printed using Agilus 30 black material, each with a thickness of 0.2 mm. These skins encase and secure the FSR sensors and are then attached to the Fin-Ray-based finger. This configuration ensures that the sensor readings are unaffected by localized, concentrated pressures and additionally provides protection against sharp objects or contamination. Moreover, as the sensor is firmly attached near the tip of the Fin-Ray finger, finite element analysis confirms that the deformation at this location is minimal under various force conditions. This negligible deformation ensures that the performance of the FSR sensor remains unaffected, allowing it to function reliably across different grasping scenarios.

Three of these commercial FSR sensing arrays (RX-M0404S) are implemented at the fingertips of the gripper. These FSRs operate on the principle of resistance variation through mechanical deformation. When external force is applied to a sensing pixel, the internal conductive filler between the pixels undergoes compression. This compression alters the contact area and distribution of the conductive filler particles, which in turn changes the electrical resistance of the pixel predictably. Each array contains 16 sensor pixels and every pixel functions as a variable resistor, which can dynamically alter its resistance based on the applied force, thereby enabling precise distributed force measurement. However, the sensor requires careful calibration, since there are factors like uniformity of the conductive filler and manufacturing errors that can influence the resistance change.

The FSR sensing system is integrated with an electronic circuit designed to sequentially activate and read each sensing unit. This is achieved using a scanning Multiplexer (MUX), specifically the CD74HC4067SM, which supplies voltage to each of the 16 sensing units (pixels) in the tactile array. The resistance of each FSR pixel, which changes based on the applied force, is then measured indirectly. A MAX11632EEGT Analogue-to-Digital Converter (ADC) is used to convert the voltage across the FSR into a digital signal. This

ADC utilizes a reference voltage as a baseline, translating the change in voltage caused by the FSR's resistance into a precise digital output. This digital signal represents the effective resistance of the FSR pixel under the applied force.

To correlate the resistance with applied force, a calibration process is employed. During calibration, known forces are applied to the FSR, and the resulting resistance changes are recorded. A linear relationship between resistance and force is established based on this data, which allows the system to interpret resistance values as corresponding normal force measurements. This step is crucial, as the inherent variability in FSR manufacturing and material properties can affect the resistance–force relationship. The detailed calibration process is introduced below.

The calibration process involves fixing the FSR sensor on a 6-axis M3813B load cell and subjecting it to a continuous load. The readings from both the FSR sensor and the load cell are recorded simultaneously. These experiments are repeated five times, and the outcomes are illustrated in Figure 4a, where the X-axis represents the Z-axis force readings from the load cell, and the Y-axis represents the average 16-pixel readings from the FSR sensor. Given that the load cell has been tested to only have a relative error of less than 0.1% in force readings, it serves as the ground truth equivalent to the generated force.

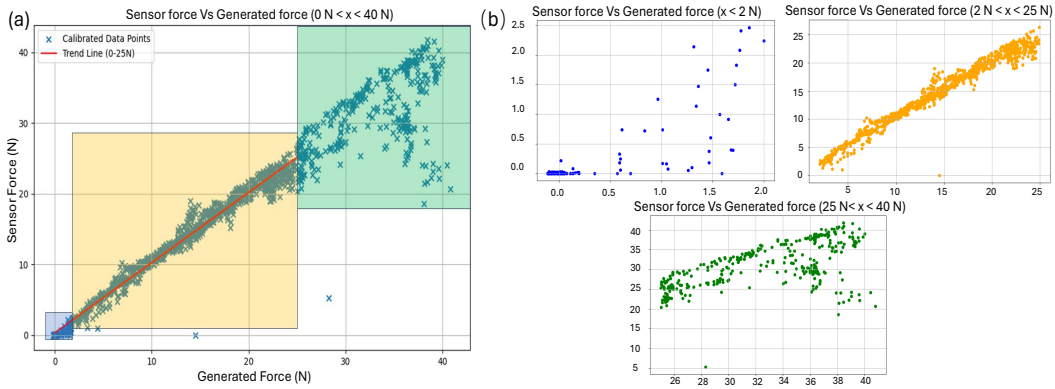


Figure 4. Calibration Results. (**a**) All data points of the FSR sensor calibration. (**b**) Sensor force vs. generated force across three distinct ranges. Its unit is the same as part (**a**).

The collected data can be categorized into three distinct ranges, represented by blue, yellow, and green, corresponding to three sensor states of the sensor shown in Figure 4b.

- Blue Range (0–2 N): 7 In this range, most FSR readings were below the actual values and close to zero. Data points show a significant variance, indicating unstable readings. As a result, the minimum detection threshold of the sensor is identified as 2 N.
- Yellow Range (2–25 N): In this range, data are highly consistent and closely aligned with true values, indicating that this range is the operational range. A linear regression trend can be used to describe this range with the equation $Y = 1.01X - 0.44$.
  - Sensitivity: 1.01
  - Offset: 0.44
  - Standard deviation: 0.11, indicating stable performance.
  - Relative accuracy: 93.41%, confirming the sensor's effectiveness within this range.
- Green Range (Above 25 N): In this range, data show significant dispersion, marking 25 N as the upper limit of the operational range.

This analysis highlights the sensor's performance across its detection spectrum, emphasizing high accuracy and stability within the yellow range.

In conclusion, the sensor's operational range is between 2 N and 25 N, with an accuracy of 93.41%. Its spatial resolution is 0.6 mm, while the temporal resolution is 67 ms. The sensitivity of the sensor is measured at 1.01, and it experiences a drift of 11%. More details regarding FSR sensor performance can be found on our project website: https://sites.google.com/view/tacfr-gripper/sensor-calibration (Accessed on 14 December 2024).

3.3. Tactile Perception for Grasping Stability Detection

Compliant grippers can easily adjust to different object shapes and sizes due to their flexibility. This reduces the need for specific control adjustments for each geometry. However, their flexibility may affect precision in placement due to deformation. Integrating tactile sensors (such as FSR sensors) with these grippers provides real-time feedback on contact information. This allows for precise control adjustments. Here, we compare two methods for tactile data interpretation and demonstrate the advantages of incorporating tactile sensors into the proposed robotic gripper.

3.3.1. Threshold-Based Method

The experiment setup is as follows: First, place an object on the fixed position for the gripper in Configuration 1 to grasp. The average force of the reading on each pixel of the FSR sensor is calculated as the contact force. The minimal contact force of the gripper required to lift the object without it falling is determined by gradually reducing the contact force until the combined support forces are less than the object's weight. This involves carefully adjusting the FSR sensor's force threshold to ensure the applied force is just enough for a stable grip without causing slippage. By systematically iterating and testing, the optimal minimum force threshold is identified, which we define as the lower threshold boundary. The upper boundary is set 2 N above the lower boundary, ensuring a stable yet responsive grip without a lengthy oscillation period or excessive force. The 2 N increment represents a relatively small range that, based on experimental results, strikes a good balance between response time and force control.

3.3.2. Human-in-the-Loop Control

The control framework of the robotic hand consists of two pathways, depicted in Figure 5a: manual control (in black) and tactile feedback (in red). In the manual control pathway, the operator sends commands via an Xbox controller, which the computer processes and forwards to an Arduino board to actuate the robotic hand. In the tactile feedback pathway, sensor data are analysed locally to determine the appropriate response, providing haptic feedback to the operator and adjusting the contact force autonomously if the closed-loop control is activated.

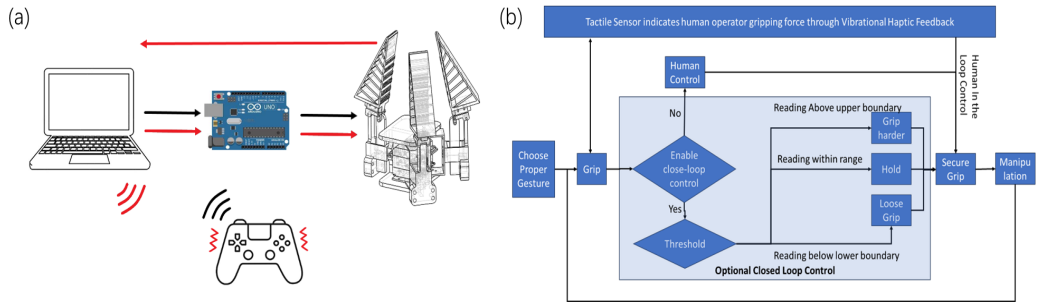


Figure 5. (**a**) Control strategy of robotic hand. (**b**) Flow chart of human-in-the-loop control strategies and threshold-based control strategies.

As shown in Figure 5b, the flowchart provides a detailed outline of both Human-in-the-Loop (HITL) control and threshold-based autonomous grasping:

HITL Control: The strength of the grip is indicated to the user through the amplitude of the controller's vibrations, providing real-time feedback on the force being applied. Threshold-Based Autonomous Grasping: During closed-loop control, the sensor readings are dynamically compared with a preset threshold range, allowing the system to automatically adjust the motor state. This adjustment includes increasing force, releasing, or holding based on real-time feedback, providing adaptive control and stabilization during grasping.

4. Experiments & Results

4.1. Gripping Capability Evaluation

The first experiment aims to assess the gripping capability. In this experiment, the gripper engages with different objects and repeatedly grasps each object ten times to evaluate the success rate across three different configurations. During these tests, the initial position of the object is maintained, but slight variations in the object's orientation are introduced to simulate real-world conditions. The properties of the objects used in the gripping experiments are summarized in Figure 6, listed from lightest to heaviest. The properties of the objects used in the gripping experiments are summarized in Table 1. The term 'Dimensions (d × h)' refers to the approximate diameter of the object multiplied by its height, with units in millimetres (mm).

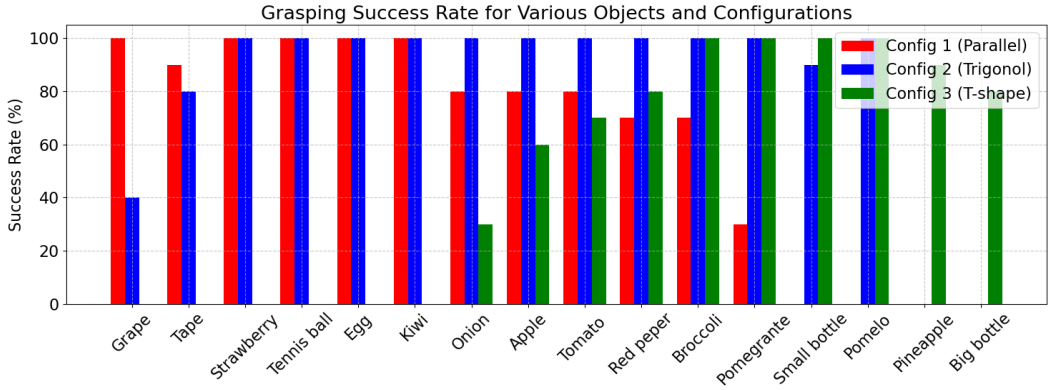


Figure 6. Success rate of grasping various objects using different gripper configurations.

Table 1. Testing objects for grasping.

Object	Weight	Dimensions (d × h)	Properties
Grape	8 g	20 mm × 26 mm	Soft, smooth
Tape	20 g	54 mm × 16 mm	Rigid, smooth
Strawberry	20 g	34 mm × 43 mm	Soft, rough
Tennis Ball	55 g	65 mm × 65 mm	Soft, rough
Egg	60 g	43 mm × 53 mm	Rigid, smooth
Kiwi	117 g	57 mm × 70 mm	Soft, rough
Onion	144 g	67 mm × 64 mm	Rigid, rough
Apple	160 g	72 mm × 67 mm	Rigid, rough
Tomato	172 g	72 mm × 64 mm	Soft, smooth
Red Pepper	200 g	86 mm × 76 mm	Soft, rough
Broccoli	375 g	110 mm × 150 mm	Rigid, rough
Pomegranate	487 g	96 mm × 86 mm	Rigid, smooth
Small Bottle	515 g	60 mm × 200 mm	Soft, smooth
Pomelo	913 g	160 mm × 150 mm	Rigid, smooth
Pineapple	1210 g	110 mm × 210 mm	Rigid, rough
Big Bottle	1540 g	80 mm × 315 mm	Soft, smooth

The results of the experiment are shown in Figure 6, where the different colours of bars represent different configurations. As indicated by the prior analysis of the workspace, the gripper encounters difficulties with objects that are either too small (less than 10 mm in

radius) or too large (exceeding 125 mm in radius) for specific configurations. To address these challenges, the gripper leverages a reconfigurable capability, selecting the optimal configuration for grasping different objects. This adaptation ensures an optimal success rate of 97.5%.

Configuration 1 excels in the manipulation of smaller objects. Configuration 2 demonstrates the best overall performance and has a high success rate in terms of grasping medium-sized objects. In contrast, Configuration 3 particularly excels in grasping larger, elongated, heavier objects. In conclusion, the gripper's morphological differences enabled by reconfigurable design significantly enhance its grasping capabilities. The gripper has been tested and is capable of grasping objects ranging from 4 mm to 80 mm in radius. It is particularly effective at handling objects with spherical or cylindrical shapes, making it highly suitable for picking up fruits and vegetables when the gripper configuration is adjusted appropriately. This adaptability is crucial in real-world scenarios where a diversity of objects demands varied manipulation strategies.

In Terrile's work [37], four distinguished soft robotic grippers are manufactured and tested for grasping a set of daily objects. These objects varied in weight, spanning a range from 7.9 g to 229.6 g.

In contrast, our experiment utilizes objects with a significantly broader weight and size range; the smallest object tested is a grape, with a diameter and height of 20 mm × 26 mm, while the largest is a water bottle measuring 80 mm × 310 mm. Experimental measurements indicate that the maximum graspable weight reaches 1540 g. This represents an increase by a factor of eight compared to the range used in the referenced study. Consequently, our dataset presents a more challenging and general spectrum for assessing the performance of soft robotic grippers.

In their study, the most efficient gripper, based on the MultiChoice Gripper product manufactured by FESTO, achieved an 89% success rate in object grasping experiments [37]. In contrast, our gripper, as illustrated in Figure 6, demonstrates variable performance depending on its configurations. Given its three distinct configurations, each optimized for objects of varying sizes, a single mode may exhibit reduced efficacy in handling objects outside its target size range. This specificity results in lower overall success rates for each mode. However, when each object is engaged using the optimal configuration, our gripper achieves an overall success rate of 97.5%. This significant improvement underscores the structural effectiveness of our gripper design.

Other experiments are carried out to evaluate how the grasping capacity changes in relation to the object's dimensions. We utilized 3D-printed circular objects made from PLA material, with diameters ranging from 10 to 150 mm to create 15 samples, as shown in Figure 7a. Each object had a fixed height of 30 mm. To standardize the testing conditions, we ensured that all objects shared consistent material properties (eSun PLA+), shape, and surface texture, minimizing the influence of external factors. At the bottom of each 3D-printed object, weights were suspended for testing varying loads. The experiment was conducted by using the gripper's different configurations to grasp each object. We gradually increased the weight until slippage occurred between the gripper and the objects. The point of slippage was recorded as the maximum load that the gripper could sustain for that specific dimension. Three tests are taken, then the average load is calculated as the final slippage point. By fixing the object's shape, stiffness, friction, and initial position, the experiment isolated the variable of object size (diameter) to explore its influence on grip strength. This experiment ensured repeatability and allowed for a more precise evaluation of the gripper's performance across its different configurations. The results from this experiment provide quantitative insights into how object size impacts gripping performance and demonstrate the effectiveness of the gripper's design under more standardized and controlled conditions.

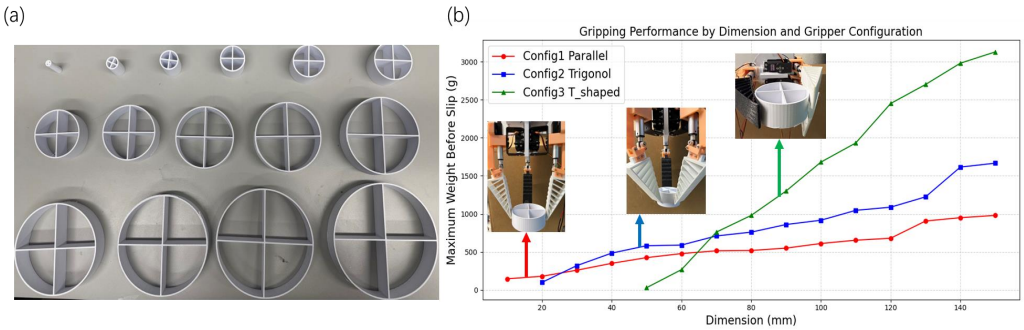


Figure 7. (**a**) 3D-printed samples for grasping test listed from 10 mm to 150 mm in diameter. (**b**) The maximum grasping load versus the sample diameter with different configurations.

Among the configurations tested, the Parallel configuration demonstrated strong performance for smaller objects (10–20 mm in diameter) due to its narrow finger spacing. However, for medium-sized objects (70 mm in diameter), the power grasp configuration demonstrated a rapid improvement in performance. This was primarily attributed to its Fin-Ray effect, which enabled the fingers to conform closely to the object's shape. This conformal contact significantly increased the effective contact area and deformation further, resulting in better grasping strength. This configuration proved particularly effective for grasping large objects due to its ability to leverage both shape adaptation and increased contact surface. Therefore, in this experiment, the maximum load the gripper could grasp was 3180 g, achieved with a 150 mm diameter object using the T-Shaped configuration

The Trigonal configuration exhibited 40.21% better overall grasping performance compared to the Parallel configuration. However, due to the placement of its grasping points near the tips of the fingers, it could not achieve the same contact area as the T-shape configuration. Worth noticing, for objects with a diameter of around 130 mm, the object diameter finally aligned with the gripper's finger spacing, leading to a significant increase in the contact area. However, unlike the T-shaped configuration, this contact area cannot expand significantly with further increases in object size, resulting in a much slower improvement in gripping performance. A video showcasing the grasping experiments can be found in the Supplementary Materials.

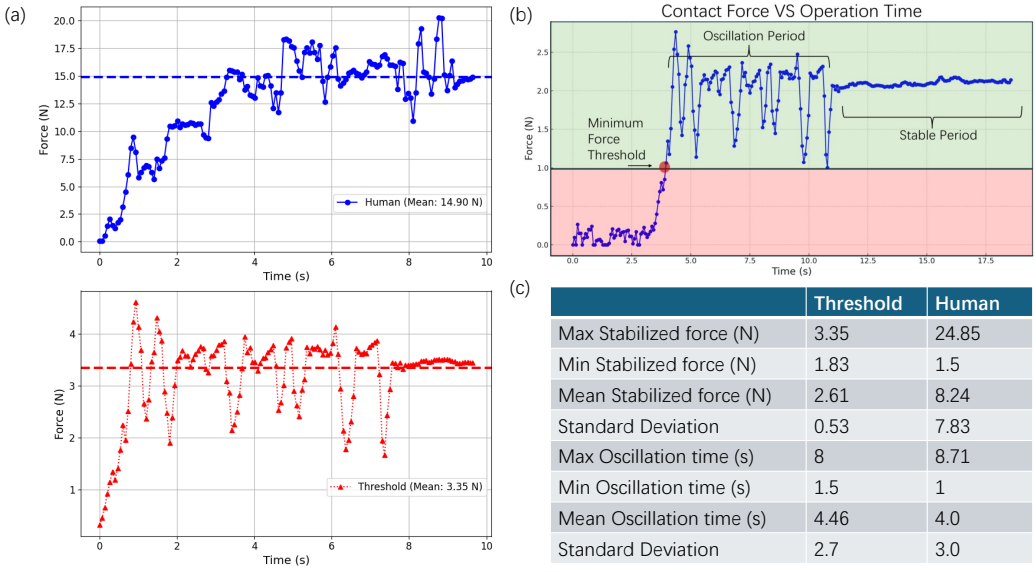
4.2. Performance Evaluation for Different Control Strategies

By equipping the gripper with FSR tactile sensors, threshold-based grasping stability detection methods are used to ensure a secure grasp on the objects while applying minimal force. The experiment involves using the TacFR-Gripper to grasp a tested object, specifically an onion in this case. The gripping force is progressively increased until the tactile sensor indicates a transition from a 'Non-Graspable' status to a 'Graspable' condition. Additionally, a HITL method is employed as the baseline, where a user controls the gripper with a remote controller and visually determines if the grasp is secure and uses the vibrational indicator on the controller to indicate how strong the grip is. Subsequently, the gripper, mounted on a robotic arm, is lifted to test if it can maintain a secure grip on the object. Ten repeated experiments are carried out to evaluate the performance of different control strategies.

Here are two important factors that are taken into consideration for evaluating the gripping performance. As Figure 8b shows, during the gripping process there are different phases of gripping state changes. It clearly illustrates the initial sensor noise (0–2.5 s), followed by an oscillation phase (4–11 s) that signifies an unstable grasp, and eventually, a stable phase (after 11 s), where readings stabilize within the established threshold. The lowest force reading observed during the oscillation phase is indicative of the minimum force threshold, which sets the lower boundary for the force threshold.

- Oscillation Time Cost: This metric measures the speed at which the gripper stabilized the successful grasping. Quick detection and response are crucial for efficient and timely robotic operations.

- Stabilized Contact Force: This metric examines the final amount of force applied during grasping to maintain a secure grip without applying excessive force, especially when manipulating delicate and soft objects.



	Threshold	Human
Max Stabilized force (N)	3.35	24.85
Min Stabilized force (N)	1.83	1.5
Mean Stabilized force (N)	2.61	8.24
Standard Deviation	0.53	7.83
Max Oscillation time (s)	8	8.71
Min Oscillation time (s)	1.5	1
Mean Oscillation time (s)	4.46	4.0
Standard Deviation	2.7	3.0

Figure 8. (**a**) Comparative analysis between the HITL control and threshold-based control. (**b**) Different periods during the grasping process. (**c**) Summary of experimental data.

The upper graph in Figure 8a is a typical force curve that demonstrates relying solely on human-in-the-loop control during teleoperation to determine the grasping state of objects, resulting in significantly higher gripping forces, averaging 15.23 N when the grasp stabilizes. Such excessive force is unacceptable, as it can easily damage delicate items. Therefore, although the TacFr gripper has a Fin-Ray structure to better conform to the objects, the grasping force can still be extremely large. Incorporating tactile feedback into the gripper is essential for effective object handling. While in the contract, the threshold control method has an average of 3.35 N gripping force when the grasp stabilizes.

Figure 8c summarizes all experimental data, revealing that, in HITL control, gripping forces are highly variable and closely related to the operator's familiarity with the system. The maximum force reached up to 25 N, while the minimum was only 1.5 N, showing a wide and scattered distribution, with a standard deviation of 7.83. Similarly, oscillation periods exhibit high variability. In contrast, the threshold control method significantly reduces this variation, with a standard deviation of only 0.53 and stabilized force values concentrated between 1.83 N and 3.35 N. Although the oscillation period under threshold control is approximately 11% higher than with manual control, this minor trade-off is acceptable for achieving better precision.

During the grasping, the threshold method relies on a fixed force threshold to determine whether or not an object is securely grasped. Each finger of the gripper adjusts its position to ensure that the force applied by each finger falls within this threshold range. However, this approach can sometimes cause the gripper to continue adjusting its fingers even after the object is securely grasped. This happens because the gripper focuses solely on meeting the force threshold criteria, potentially overlooking the fact that the object is already held firmly, albeit in a slightly different position or orientation than originally intended (i.e., the position or orientation expected when the threshold values were manually set). This constant adjustment can lead to inefficiencies, in particular, longer adjustment periods (as shown by the oscillation period in Figure 8b). While the extended adjustment time can be mitigated by broadening the force range used in the threshold method, this also increases the upper boundary of force applied to the objects. This necessitates a trade-off and extensive fine-tuning to achieve a balance between efficiency and applied force.

In contrast, for HITL grasping, the operator can both feel the gripping force and visually observe the grasping state. Unlike the threshold method, where continuous fine-tuning is needed to meet the pre-set force range, an operator can directly judge grasp success based on visual feedback. This is why HITL control is slightly more efficient in terms of response time compared to the threshold-controlled gripper.

Such decreased gripping force demonstrates operational efficiency and several advantages, including a lower risk of damaging objects and enhanced energy efficiency.

4.3. Evaluation of In-Hand Manipulation

To further emphasize the dexterity of our experimental gripper, we conducted an experiment to evaluate how effectively the gripper could adjust the position of various everyday objects while maintaining a secure grip.

In the physical experiment, the object is placed at the centre of the gripper, which then moves the object to the right as far as possible. By tracking and measuring the displacement at the object centre points, we could determine the maximum lateral displacement occurring during the in-hand manipulation process. The results in Figure 9a show that the manipulability range (ΔX) varied for different objects.

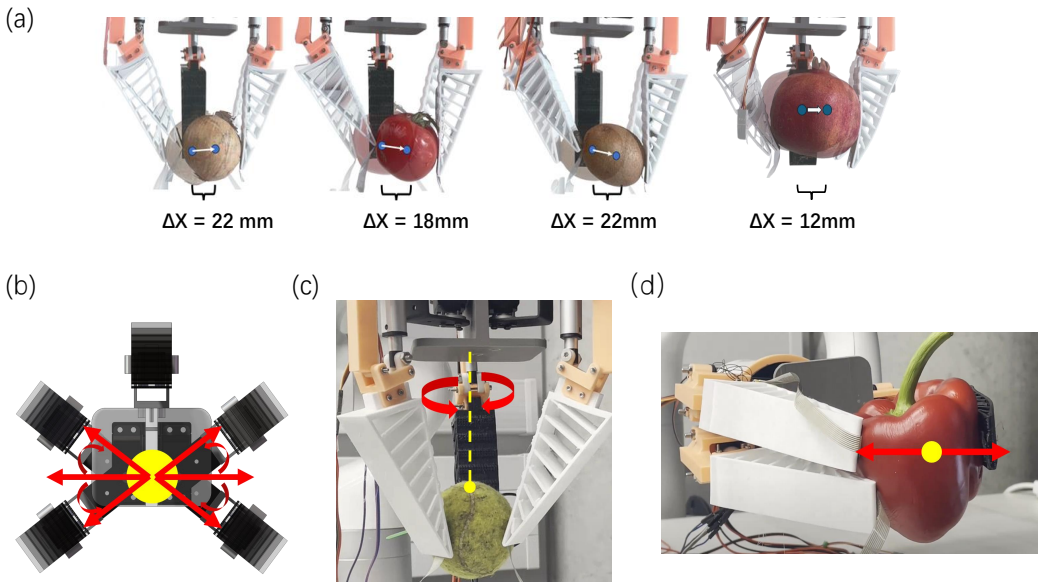


Figure 9. (**a**) The physical experimental results for manipulating objects with various sizes and shapes. ΔX indicates the maximum in-hand object translation distance. (**b**) Object lateral manipulation with the aid of servo motor. (**c**) Object rotational manipulation. (**d**) Object lateral manipulation in the power grasp configuration.

As Figure 9b shows, the integration of the base servo motor allows the gripper to manipulate objects over an extra 60° range. When the servo motor is fixed, the gripper can move objects laterally in a plane. However, if the servo motor is not fixed, the entire plane can be rotated approximately plus/minus 30 degrees, allowing for a much larger manipulation range, which significantly enhances the gripper's versatility.

Moreover, the gripper is equipped with a third finger, which, although fixed, works in conjunction with the other two fingers to perform partial rotational operations within the palm, as shown in Figure 9c, and lateral movement in the power grasp configuration, as shown in Figure 9d. This coordination between the fingers enables more complex in-hand manipulations, further showcasing the gripper's potential in in-hand manipulation tasks. For a detailed visualization of the manipulation experiment, refer to the Supplementary Materials.

5. Discussion and Conclusions

In this paper, we introduce the TacFR-Gripper, a reconfigurable Fin-Ray-based soft tactile gripper capable of grasping and manipulating objects of various sizes. We incorporated a tactile sensor array onto the soft Fin-Ray finger, which is known as the tactile skin. We utilize a threshold-based force control strategy for tactile data processing, significantly enhancing the gripper's grasp detection capabilities. Through rigorous testing and comprehensive analysis, we demonstrate the TacFR-Gripper's proficiency in handling a wide range of delicate objects, showcasing its potential dexterity for in-hand manipulation. The modular design of the finger and the gripper base allows the fingers to be replaced without disassembling the entire gripper, which has greatly improved the efficiency of performance testing with different finger designs. Nevertheless, this work has areas for further improvement. In our future work, we plan to integrate both vision and tactile sensing across the entire gripper surface, enabling more precise environmental perception and complex manipulation strategies.To comprehensively evaluate the TacFR-Gripper's capabilities, we will develop and conduct more complex tasks involving contact-rich dexterous manipulation. Additionally, we aim to refine workspace simulation by incorporating key parameters such as weight, friction, geometric shape, and deformation of the gripper itself into the simulation for greater accuracy. Moreover, more studies should be conducted to compare the proposed gripper with other soft grippers, allowing us to further investigate its grasping performance and adaptability in varied scenarios. Furthermore, in order to improve the grasping strategies, we plan to incorporate new algorithms such as Graph Convolutional Networks for processing the tactile sensor data, thereby enabling a more intelligent interpretation of the contact information and real-time grasping adjustment. Furthermore, topology optimization workflows are required to further improve the design of the robotic grippers with different specific application scenarios. We believe that those advancements will not only enhance the gripper's versatility and robustness but also contribute to the broader development of soft grippers integrating tactile information for better manipulation in unstructured environments.

Supplementary Materials: The following supporting information can be found at the provided links:

- General Performance: https://www.youtube.com/watch?v=KzrhTUUVxxM (accessed on 14 December 2024).
- FEM Analysis: https://www.youtube.com/watch?v=0XKuna0Az5M (accessed on 14 December 2024).
- Grasping Video: https://www.youtube.com/watch?v=mV0d4iYhEi8 (accessed on 14 December 2024).
- Manipulation Video: https://www.youtube.com/watch?v=BKBk642TVG4 (accessed on 14 December 2024).

Author Contributions: Conceptualization, D.Z.; methodology, Q.C.; software, W.F. and Q.C.; validation, Q.C., D.Z. and W.F.; formal analysis, Q.C.; resources, D.Z.; writing—original draft preparation, Q.C.; writing—review and editing, W.F. and D.Z.; supervision, D.Z.; project administration, D.Z. All authors have read and agreed to the published version of the manuscript.

Funding: This research received no external funding.

Data Availability Statement: The data supporting the reported results in this study are available at our project website: https://sites.google.com/view/tacfr-gripper/homepage (accessed on 14 December 2024).

Conflicts of Interest: The authors declare no conflicts of interest.

Abbreviations

The following abbreviations are used in this manuscript:

HILT	Human-in-the-Loop
FSR	Force-Sensing Resistor

References

1. Alves, S.; Babcinschi, M.; Silva, A.; Neto, D.; Fonseca, D.; Neto, P. Integrated design fabrication and control of a bioinspired multimaterial soft robotic hand. *Cyborg Bionic Syst.* **2023**, *4*, 0051. [CrossRef]
2. Silva, A.; Fonseca, D.; Neto, D.; Babcinschi, M.; Neto, P. Integrated design and fabrication of pneumatic soft robot actuators in a single casting step. *Cyborg Bionic Syst.* **2024**, *5*, 0137. [CrossRef]
3. Crooks, W.; Vukasin, G.; O'Sullivan, M.; Messner, W.; Rogers, C. Fin ray effect inspired soft robotic gripper: From the RoboSoft grand challenge toward optimization. *Front. Robot.* **2016**, *3*, 70. [CrossRef]
4. Almanzor, E.; Thuruthel, T.; Iida, F. Automated fruit quality testing using an electrical impedance tomography-enabled soft robotic gripper. In Proceedings of the 2022 IEEE/RSJ International Conference on Intelligent Robots and Systems (IROS), Kyoto, Japan, 23–27 October 2022; pp. 8500–8506. [CrossRef]
5. Dong, H.; Bozkurttas, M.; Mittal, R.; Madden, P.; Lauder, G. Computational modelling and analysis of the hydrodynamics of a highly deformable fish pectoral fin. *J. Fluid Mech.* **2010**, *645*, 345–373. [CrossRef]
6. Ali, M.; Zhanabayev, A.; Khamzhin, S.; Mussin, K. Biologically inspired gripper based on the Fin-Ray effect. In Proceedings of the 2019 5th International Conference on Control, Automation and Robotics (ICCAR), Beijing, China, 19–22 April 2019; pp. 865–869. [CrossRef]
7. Shintake, J.; Cacucciolo, V.; Floreano, D.; Shea, H. Soft robotic grippers. *Adv. Mater.* **2018**, *30*, 1707035. [CrossRef] [PubMed]
8. Bullock, I.; Dollar, A. Classifying human manipulation behavior. In Proceedings of the 2011 IEEE International Conference on Rehabilitation Robotics (ICORR), Zurich, Switzerland, 29 June–1 July 2011; pp. 1–6. [CrossRef]
9. Lu, Q.; Baron, N.; Clark, A.; Rojas, N. Systematic object-invariant in-hand manipulation via reconfigurable underactuation: Introducing the RUTH gripper. *Int. J. Robot. Res.* **2021**, *40*, 1402–1418. [CrossRef]
10. Cai, Y.; Yuan, S. In-hand manipulation in power grasp: Design of an adaptive robot hand with active surfaces. In Proceedings of the 2023 IEEE International Conference on Robotics and Automation (ICRA), London, UK, 29 May–2 June 2023; pp. 10296–10302.
11. Sakuma, T.; Von Drigalski, F.; Ding, M.; Takamatsu, J.; Ogasawara, T. A universal gripper using optical sensing to acquire tactile information and membrane deformation. In Proceedings of the 2018 IEEE/RSJ International Conference on Intelligent Robots and Systems (IROS), Madrid, Spain, 1–5 October 2018; pp. 1–9.
12. Zhang, X.; Yang, T.; Zhang, D.; Lepora, N. TacPalm: A Soft Gripper with a Biomimetic Optical Tactile Palm for Stable Precise Grasping. *IEEE Sens. J.* **2024**, *24*, 38402–38416. [CrossRef]
13. Li, S.; Yin, X.; Xia, C.; Ye, L.; Wang, X.; Liang, B. TaTa: A universal jamming gripper with high-quality tactile perception and its application to underwater manipulation. In Proceedings of the 2022 International Conference on Robotics and Automation (ICRA), Philadelphia, PA, USA, 23–27 May 2022; pp. 6151–6157. [CrossRef]
14. Zhao, J.; Adelson, E. GelSight Svelte: A human finger-shaped single-camera tactile robot finger with large sensing coverage and proprioceptive sensing. *arXiv* **2023**, arXiv:2309.10885.
15. Chen, G.; Tang, S.; Xu, S.; Guan, T.; Xun, Y.; Zhang, Z.; Wang, H.; Lin, Z. Intrinsic Contact Sensing and Object Perception of an Adaptive Fin-Ray Gripper Integrating Compact Deflection Sensors. *IEEE Trans. Robot.* **2023**, *39*, 4482–4499. [CrossRef]
16. Yuan, W.; Dong, S.; Adelson, E. Gelsight: High-resolution robot tactile sensors for estimating geometry and force. *Sensors* **2017**, *17*, 2762. [CrossRef] [PubMed]
17. Liu, S.; Adelson, E. GelSight Fin Ray: Incorporating tactile sensing into a soft compliant robotic gripper. In Proceedings of the 2022 IEEE 5th International Conference on Soft Robotics (RoboSoft), Edinburgh, UK, 4–8 April 2022; pp. 925–931. [CrossRef]
18. Fan, W.; Li, H.; Si, W.; Luo, S.; Lepora, N.; Zhang, D. ViTacTip: Design and verification of a novel biomimetic physical vision-tactile fusion sensor. *arXiv* **2024**, arXiv:2402.00199.
19. Li, R.; Peng, B. Implementing monocular visual-tactile sensors for robust manipulation. *Cyborg Bionic Syst.* **2022**, *2022*, 9797562. [CrossRef] [PubMed]
20. Fan, W.; Li, H.; Xing, Y.; Zhang, D. Design and evaluation of a rapid monolithic manufacturing technique for a novel vision-based tactile sensor: C-Sight. *Sensors* **2024**, *24*, 4603. [CrossRef]
21. Yang, Y.; Jin, K.; Zhu, H.; Song, G.; Lu, H.; Kang, L. A 3D-Printed Fin Ray Effect Inspired Soft Robotic Gripper with Force Feedback. *Micromachines* **2021**, *12*, 1141. [CrossRef] [PubMed]
22. Chen, K.; Li, T.; Yan, T.; Xie, F.; Feng, Q.; Zhu, Q.; Zhao, C. A soft gripper design for apple harvesting with force feedback and fruit slip detection. *Agriculture* **2022**, *12*, 1802. [CrossRef]
23. Low, J.; Khin, P.; Han, Q.; Yao, H.; Teoh, Y.; Zeng, Y.; Li, S.; Liu, J.; Liu, Z.; Valdivia y Alvarado, P. Sensorized reconfigurable soft robotic gripper system for automated food handling. *IEEE/ASME Trans. Mechatron.* **2021**, *27*, 3232–3243. [CrossRef]
24. Sheng, X.; Li, J.; Zhang, Y.; Yang, Y.; Liu, J.; Liu, Z. Adaptive wrapping with active elastic band-based gripper for stable in-hand manipulation. *Sens. Actuators Phys.* **2024**, *377*, 115743. [CrossRef]
25. Li, S.; Wan, F.; Song, C. Active Surface with Passive Omni-Directional Adaptation for In-Hand Manipulation. In Proceedings of the 6th International Conference on Reconfigurable Mechanisms and Robots (ReMAR), Chicago, IL, USA, 23–26 June 2024, pp. 627–632. [CrossRef]
26. Wang, H.; Gao, B.; Hu, A.; Xu, W.; Shen, H.; He, J. Design of a Reconfigurable Gripper with Rigid-Flexible Variable Fingers. *IEEE/ASME Trans. Mechatron.* **2024**, 1–12. [CrossRef]
27. Batsuren, K.; Yun, D. Soft robotic gripper with chambered fingers for performing in-hand manipulation. *Appl. Sci.* **2019**, *9*, 2967. [CrossRef]

28. Pagoli, A.; Chapelle, F.; Corrales, J.; Mezouar, Y.; Lapusta, Y. A soft robotic gripper with an active palm and reconfigurable fingers for fully dexterous in-hand manipulation. *IEEE Robot. Autom. Lett.* **2021**, *6*, 7706–7713. [CrossRef]
29. Jain, S.; Stalin, T.; Subramaniam, V.; Agarwal, J.; Valdivia y Alvarado, P. A soft gripper with retractable nails for advanced grasping and manipulation. In Proceedings of the 2020 IEEE International Conference on Robotics and Automation (ICRA), Paris, France, 31 May–31 August 2020; pp. 6928–6934. [CrossRef]
30. Manoonpong, P.; Rajabi, H.; Larsen, J.; Raoufi, S.; Asawalertsak, N.; Homchanthanakul, J.; Tramsen, H.; Darvizeh, A.; Gorb, S. Fin ray crossbeam angles for efficient foot design for energy-efficient robot locomotion. *Adv. Intell. Syst.* **2022**, *4*, 2100133. [CrossRef]
31. Zhang, D.; Liu, J.; Gao, A.; Yang, G.Z. An ergonomic shared workspace analysis framework for the optimal placement of a compact master control console. *IEEE Robot. Autom. Lett.* **2020**, *5*, 2995–3002. [CrossRef]
32. Dai, J.; Wang, D.; Cui, L. Orientation and workspace analysis of the multifingered metamorphic hand—Metahand. *IEEE Trans. Robot.* **2009**, *25*, 942–947. [CrossRef]
33. Zhang, D.; Liu, J.; Zhang, L.; Yang, G.Z. Design and verification of a portable master manipulator based on an effective workspace analysis framework. In Proceedings of the 2019 IEEE/RSJ International Conference on Intelligent Robots and Systems (IROS), Macau, China, 3–8 November 2019; pp. 417–424.
34. Li, J.; Zhao, F.; Li, X.; Li, J. Analysis of robotic workspace based on Monte Carlo method and the posture matrix. In Proceedings of the 2016 IEEE International Conference on Control and Robotics Engineering (ICCRE), Singapore, 2–4 April 2016; pp. 1–5. [CrossRef]
35. Zhang, D.; Cursi, F.; Yang, G.Z. Wsrender: A workspace analysis and visualization toolbox for robotic manipulator design and verification. *IEEE Robot. Autom. Lett.* **2019**, *4*, 3836–3843. [CrossRef]
36. Parzen, E. On Estimation of a Probability Density Function and Mode. *Ann. Math. Stat.* **1962**, *33*, 1065–1076. [CrossRef]
37. Terrile, S.; Argüelles, M.; Barrientos, A. Comparison of Different Technologies for Soft Robotics Grippers. *Sensors* **2021**, *21*, 3253. [CrossRef] [PubMed]

Disclaimer/Publisher's Note: The statements, opinions and data contained in all publications are solely those of the individual author(s) and contributor(s) and not of MDPI and/or the editor(s). MDPI and/or the editor(s) disclaim responsibility for any injury to people or property resulting from any ideas, methods, instructions or products referred to in the content.